Impacts of wind farms on surface air temperatures

Somnath Baidya Roy[1] and Justin J. Traiteur

Department of Atmospheric Sciences, University of Illinois, 105 South Gregory Street, Urbana, IL 61820

Edited* by Stephen H. Schneider, Stanford University, Stanford, CA, and approved August 13, 2010 (received for review January 15, 2010)

Utility-scale large wind farms are rapidly growing in size and numbers all over the world. Data from a meteorological field campaign show that such wind farms can significantly affect near-surface air temperatures. These effects result from enhanced vertical mixing due to turbulence generated by wind turbine rotors. The impacts of wind farms on local weather can be minimized by changing rotor design or by siting wind farms in regions with high natural turbulence. Using a 25-y-long climate dataset, we identified such regions in the world. Many of these regions, such as the Midwest and Great Plains in the United States, are also rich in wind resources, making them ideal candidates for low-impact wind farms.

impact assessment | regional climate model | sustainable energy | wind energy | wind power potential

Wind power is one of the fastest growing energy sources in the world. Most of this growth is in the industrial sector based on large utility-scale wind farms (1). Recent studies have investigated the possible impacts of such wind farms on global and local weather and climate. Although debates exist regarding the global-scale effects of wind farms (2–5), modeling studies agree that wind farms can significantly affect local-scale meteorology (6, 7). However, these studies are based only on model simulations and are not validated against observational evidence. In this paper, we used field data and numerical experiments with a regional climate model to answer the following critical questions arising from the prior studies:

i. Does observational evidence show that wind farms affect near-surface air temperatures?
ii. Can atmospheric models replicate the observed patterns of near-surface air temperatures within wind farms?
iii. How can these impacts be minimized to ensure long-term sustainability of wind power?

Observed Impacts of Wind Farms

Although observed data on wind speed and turbulence in and around operational wind farms are readily available, information on other meteorological variables do not exist in the public domain. The only available information is temperature data from a wind farm at San Gorgonio, California, collected during June 18–August 9, 1989 (Fig. 1). To the best of our knowledge, this is the only meteorological field campaign conducted in an operational wind farm. The wind farm consisted of 23-m-tall turbines with 8.5-m-long rotor blades arranged in 41 rows that were spaced 120 m apart.

Data from the field campaign show that near-surface air temperatures downwind of the wind farm are higher than upwind regions during night and early morning hours, whereas the reverse holds true for the rest of the day (Fig. 2*A*). Thus, this wind farm has a warming effect during the night and a cooling effect during the day. The observed temperature signal is statistically significant for most of the day according to the results of a Mann–Whitney Rank Sum Test (Table 1).

A possible explanation for this phenomenon can be drawn from the hypothesis proposed by Baidya Roy et al. that turbulence generated in the wake of the rotors enhance vertical mixing (6). In a stable atmosphere when the lapse rate is positive, i.e., a warm layer overlies a cool layer, enhanced vertical mixing mixes warm air down and cold air up, leading to a warming near the surface. In an unstable atmosphere with negative lapse rate, i.e., cool air lying over warmer air, turbulent wakes mix cool air down and warm air up, producing a cooling near the surface. Vertical profiles of temperatures from the Edwards Air Force Base corroborate this hypothesis. This base is the World Meteorological Organization (WMO) recognized weather station nearest to the San Gorgonio wind farm. Data show a positive lapse rate at 4 AM and negative lapse rates at 10 AM and 4 PM at the base during the field campaign (Fig. 2*B*). The corresponding temperature signal from the San Gorgonio wind farm (Fig. 2*A*) shows a warming effect at 4 AM but a cooling effect at 10 AM and 4 PM. This pattern is consistent with the proposed hypothesis.

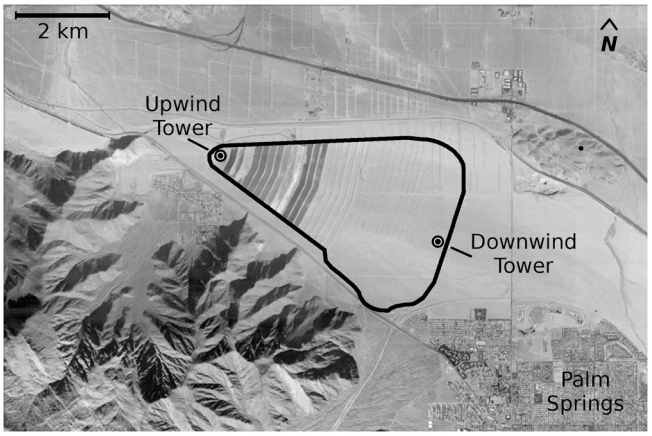


Fig. 1. Google Earth map of San Gorgonio area showing the wind farm boundary in 1989 and locations of upwind and downwind meteorological towers. The wind farm layout has changed significantly since then. Many of the small turbines from the original site have been removed and a large number of taller, more modern turbines have been added. The new turbines to the north of the old wind farm are clearly visible in the image.

Simulated Impacts of Wind Farms

We conducted a set of 306 simulations to test if regional climate models are capable of replicating the observed patterns of local warming/cooling under positive/negative lapse rates. Using the Regional Atmospheric Modeling System (RAMS) (8, 9), we simulated a small wind farm consisting of a 7×3 array of wind turbines. Each turbine was 100-m tall with 50 m rotor blades (100 m rotor diameter), spaced 10 rotor diameters, i.e., 1 km apart in both x and y directions. Wind turbine rotors were represented as elevated sinks of momentum and sources of turbulence (6). We initialized the model with atmospheric sounding data for February 1, May 1, and August 1, 2009 and November 1, 2008, from 21 WMO stations in the western United States (Table 2). These soundings collectively represent the wide range of possible stability conditions over the entire annual cycle. With each of the 153 available soundings, we conducted a pair of 1-h-long simulations: a control case and a wind farm case with the wind turbine

Author contributions: S.B.R. designed research; S.B.R. performed research; S.B.R. and J.J.T. analyzed data; and S.B.R. wrote the paper.

The authors declare no conflict of interest.

*This Direct Submission article had a prearranged editor.

[1]To whom correspondence should be addressed. E-mail: sbroy@atmos.uiuc.edu.

Downloaded by guest on March 25, 2020

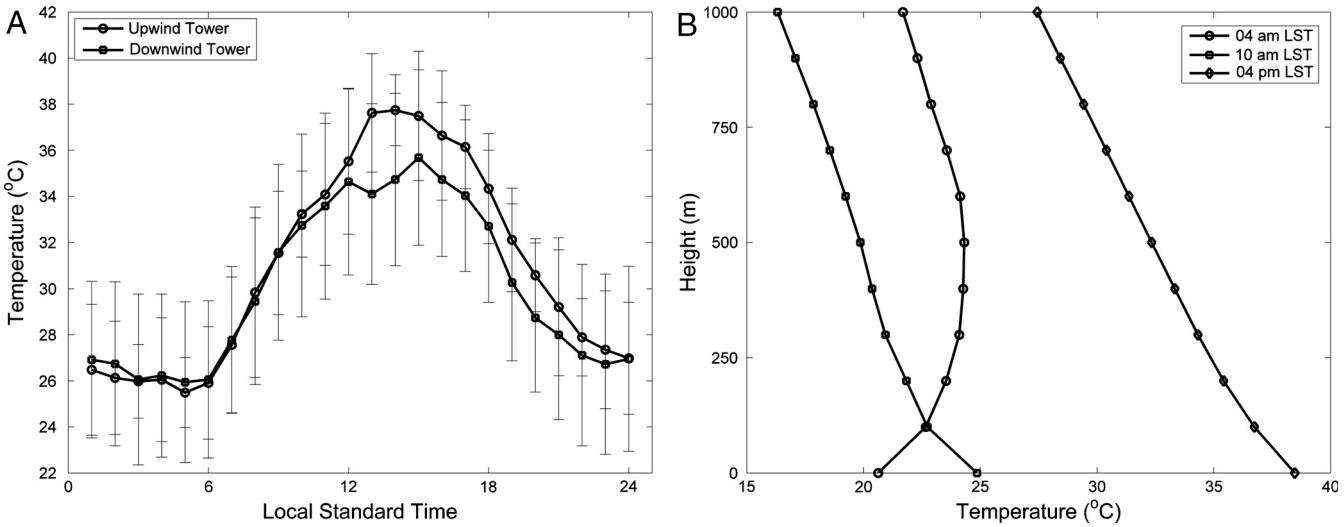


Fig. 2. Observed temperature in and near the San Gorgonio wind farm. (*A*) Near-surface air-temperature patterns at the San Gorgonio wind farm during the field campaign. (*B*) Vertical profiles of air temperature at Edwards Air Force Base during June–August 1989.

parameterization turned off and on, respectively. Typically, the atmospheric boundary layer (ABL) responds to external perturbations within a timescale of 1 h (10). Hence, these 153-h-long simulations can provide a large ensemble for a robust statistical analysis of rotor-ABL interactions. We conducted a pairwise comparison of the wind farm and control cases to quantitatively estimate the effect of wind farms on near-surface air temperatures under different stability conditions.

Fig. 3*A* shows a scatter plot of the change in the near-surface air temperature (wind farm–control) under different environmental lapse rates. The lapse rate was calculated as the average vertical gradient of potential temperature between the surface and 300 m altitude at the beginning of the simulations. It is clear from the figure that our simulations can capture the basic pattern of temperature change observed in the San Gorgonio wind farm. All the model realizations almost exclusively lie in the first and third quadrant, indicating that wind turbine rotors create a warming under positive lapse rates and a cooling under negative lapse rates. The range of observed wind speeds is much wider under stable conditions. Consequently, there is more scatter in δT under positive lapse rates.

The temperature change in wind farms was also a function of the mean ambient hub-height (second atmospheric layer) wind speed (Fig. 3*B*). The temperature signal can be approximated as a Gaussian function of hub-height wind speed, becoming zero at speeds less than 2 m/s or greater than 20 m/s and peaking at approximately 12 m/s. There are two factors that lead to weaker impacts at high wind speeds. First, at wind speeds higher than 20 m/s, the rotors are designed to stop working. If the 1-h mean wind speed is high, quite likely the instantaneous wind speeds frequently exceeded the 20 m/s limit. Hence, in those cases, the rotors worked only intermittently thereby reducing the mean impacts on the surface temperatures. Second, at high wind speeds, ambient turbulence is also high, resulting in lower impacts. This phenomenon is evident in the δT vs. ambient turbulent kinetic energy (TKE) plot (Fig. 3*C*). Ambient TKE was

Table 1. Statistical significance from Mann–Whitney Rank sum test of warming/cooling signal at downwind tower in comparison with upwind tower

LST	δT	Statistical significance, %
01	Warmer	90
02	Warmer	95
03	Warmer	Not significant
04	Warmer	95
05	Warmer	Not significant
06	Warmer	95
07	Warmer	90
08	Cooler	Not significant
09	Warmer	Not significant
10	Cooler	Not significant
11	Cooler	Not significant
12	Cooler	Not significant
13	Cooler	>99
14	Cooler	>99
15	Cooler	>99
16	Cooler	>99
17	Cooler	90
18	Cooler	>99
19	Cooler	>99
20	Cooler	90
21	Cooler	90
22	Cooler	Not significant
23	Cooler	Not significant
24	Cooler	Not significant

Any value less than 90% is considered not significant. LST, local standard time.

Table 2. Sounding data from the following WMO stations were used to initialize the RAMS model

Station	Latitude Longitude
Albuquerque, NM	35/02N 106/37W
Boise, ID	43/34N 116/13W
Denver Int Apt, CO	39/46N 104/52W
Desert Rock, NV	36/37N 116/01W
Elko, NV	40/52N 115/44W
Flagstaff, AZ	35/14N 111/49W
Glasgow, MT	48/13N 106/37W
Grand Junction, CO	39/07N 108/32W
Great Falls, MT	47/27N 111/23W
Medford, OR	42/23N 122/53W
Oakland, CA	37/45N 122/13W
Quillayute, WA	47/47N 124/33W
Reno, NV	39/34N 119/48W
Riverton, WY	43/04N 108/29W
Salem, OR	44/55N 123/01W
Salt Lake City, UT	40/47N 111/57W
San Diego, CA	32/50N 117/07W
Santa Teresa, NM	31/52N 106/42W
Spokane, WA	47/38N 117/32W
Tucson, AZ	32/07N 110/56W
Vandenberg AFB, CA	34/44N 120/33W

Downloaded by guest on March 25, 2020

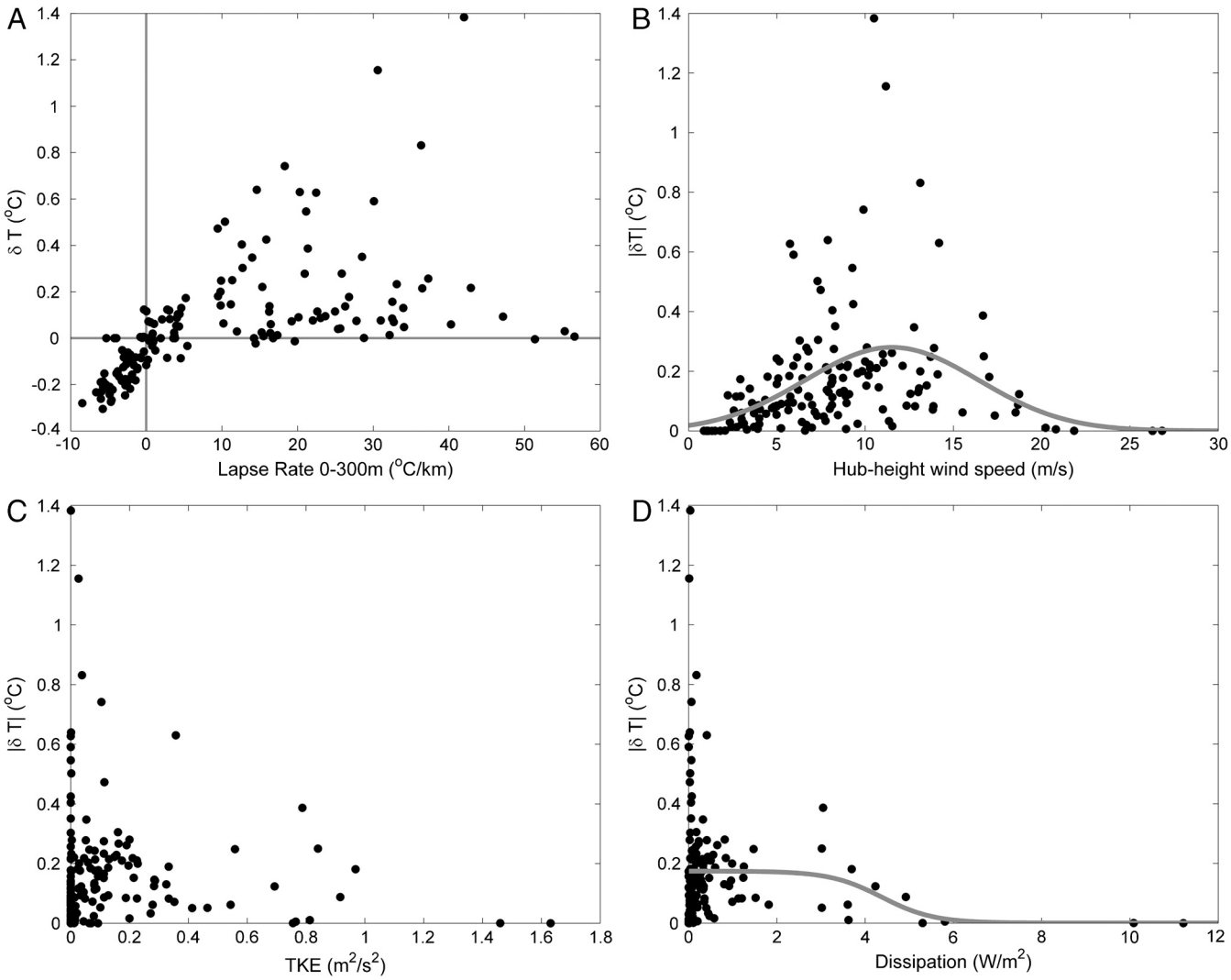


Fig. 3. Simulated change in near-surface air temperatures within the wind farm plotted as a function of (*A*) 0–300 m potential temperature lapse rate at the beginning of the simulations; (*B*) mean background hub-height (100 m) wind speed; (*C*) mean background lower ABL (0–300 m) TKE; and (*D*) mean background surface KE dissipation rate. The variables plotted on the abscissa are from the control simulations, whereas the variables on the ordinate are the difference between the control and wind farm simulations. The temperature change within the wind farm, wind speed, TKE, and surface KE dissipation rates are averaged over the entire 1-h-long simulation period for the 21 grid cells containing the turbines.

calculated by averaging the TKE in the lowest four atmospheric layers in the control runs. Fig. 3*C* shows that the temperature effects are large when ambient TKE is small and vice versa. This phenomenon implies that if the ambient environment is turbulent, the temperature profiles are well mixed and additional mixing by rotor-turbulence does not have a strong impact.

Because atmospheric turbulence is a key predictor of surface kinetic energy (KE) dissipation rate, the impacts of the rotors are strong when background surface KE dissipation rate is weak and vice versa (Fig. 3*D*). A sigmoid curve fitted to the scatter plot indicates that the impact of the rotors starts to decrease as the dissipation rate becomes larger than 2.7 W/m^2 and becomes almost zero at dissipation rates higher than 6 W/m^2.

Low-Impact Wind Farms

Based on our understanding of how wind farm rotors interact with the ABL flow, we can envisage two distinct strategies to minimize the impacts of wind farms on surface temperature. One option would be to reduce the turbulence generated by rotors. It is evident from the simulations that the turbulent rotor wakes play a key role in determining how wind farms affect the ABL. To further explore the role of rotor-generated turbulence, we conducted a series of sensitivity experiments with the TKE added by rotors set to 0, 0.5, 1, 2, 5, 10, and 15 $m^2 s^{-2}$. We ran an ensemble of 153 simulations for each case with initial conditions from WMO soundings. Fig. 4*A* shows that rotors that generate more turbulence in their wakes are likely to have a stronger impact on near-surface air temperatures.

Rotor-generated turbulence also affects the KE absorbed by the downstream wind turbines (Fig. 4*B*). The energy required to generate this turbulence comes from the KE of the mean flow. Consequently, rotors that generate more turbulence in their wakes further reduce the KE available to downstream turbines. Thus, designing new rotors that generate less turbulence in their wakes also increases the productivity of wind farms.

One interesting feature in Fig. 4*B* is that power absorbed increases for TKE values between 0 and 0.5 $m^2 s^{-2}$ but decreases thereafter. This phenomenon indicates that a small amount of turbulence in the wake is actually beneficial for wind farm operations. Wake turbulence triggers entrainment of KE from above to replenish the KE deficit in the wakes. However, there is a limit to this benefit. Rotors that generate more than 0.5 $m^2 s^{-2}$ of TKE

Downloaded by guest on March 25, 2020

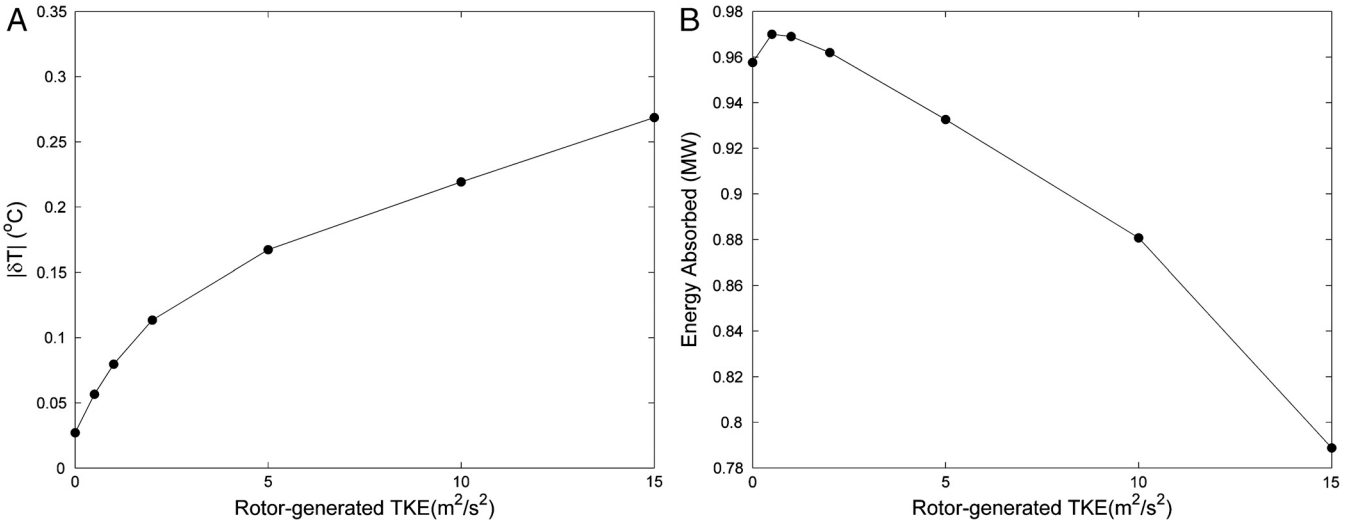


Fig. 4. Impact of wake turbulence on wind farms. (*A*) Change in near-surface air temperature within the wind farm and (*B*) mean energy absorbed by each rotor as a function of rotor-generated turbulence.

consume more KE than that replenished by entrainment. Hence, wind farms built with such rotors are less productive.

An alternative option to designing low-turbulence rotors would be to look for an optimal siting solution. The results of the numerical experiments indicate that the impacts of wind farms are likely to be small in regions where background ABL turbulence is high due to natural reasons. It is impossible to identify such regions with global long-term climatological data because data on ABL turbulence are limited. Instead we identified these regions by considering the surface KE dissipation rates. KE in atmospheric flow exists at a wide range of spatial scales. However, this KE is dissipated only at extremely small scales, mostly near the surface. ABL turbulence accelerates surface KE dissipation by breaking down large-scale flow into successively smaller and smaller eddies (11). Hence, surface KE dissipation can act as an indicator of ABL turbulence. Indeed, the simulated ABL TKE and surface KE dissipation rates are strongly correlated with $r = 0.9475$ ($P < 0.00001$). Also, the temperature signal exhibits similar relationships with ABL TKE and surface KE dissipation rate (Fig. 3 *C* and *D*).

We calculated surface KE dissipation rate for global land surface using the JRA25 dataset (12). This dataset is a 25-y-long (1979–2004), six-hourly dataset aggregated onto a $2.5 \times 2.5°$ grid using data from a wide range of sources including surface stations, meteorological towers, radiosondes, and satellites. With 41 levels in the vertical, this dataset has a higher vertical spatial resolution than other reanalysis datasets, making it the most appropriate for our analysis. According to our estimate, the global average surface KE dissipation is 2.1 W/m^2. This value corresponds well with another study using a different method from other reanalyses data (13).

Fig. 5 shows the surface KE dissipation rates averaged over the 1979–2004 period. We know from Fig. 3*D* that the impact of wind farms starts decreasing sharply as ambient surface KE dissipation rate becomes larger than 2.7 W/m^2 and becomes almost zero at dissipation rates higher than 6 W/m^2. Expectedly, the surface KE dissipation is high in regions with high topography like the Rockies, Andes, Himalayas, and the Tibetan Plateau. Due to their relative inaccessibility, these regions are not suitable for wind farms. Same consideration eliminates Greenland and Antarctica as candidates. However, large parts of North and Central America, the southern tip of South America, northern Europe, Russia, northern China, the Rift Valley, and southern parts of Africa, southern Australia, and New Zealand seem to be ideal for low-impact wind farms.

This analysis identifies regions where wind farms are likely to generate lower impacts on near-surface air temperatures. The map in Fig. 5 has considerable overlaps with the wind resources map shown in figure 1 of Lu et al. (14). For example, in the United States, the Great Plains and the Midwest regions seem to be ideal for harvesting wind energy because wind farms in these wind-rich regions are likely to produce relatively less impacts on surface temperatures.

Both the engineering and siting solutions have pros and cons. The engineering solution is expensive because it involves designing new rotors. However, it is particularly attractive because, apart from minimizing impacts, it will improve the productivity of the wind farm. Additionally, it will also reduce structural damage to turbines from turbulence in the wakes of upstream rotors (15, 16). On the other hand, the siting solution is convenient because it can be implemented with currently available technology. However, it requires wind farms to be sited in regions with high background ABL turbulence. Background turbulence is generally weaker than wake turbulence but prolonged exposure may be damaging to the rotors (15).

Discussion

This study has significant implications for future energy and land use policy. Wind power can be a part of the solution to the atmospheric carbon problem (17). Acknowledging the potential of wind energy, all large industrial economies are prominently featuring wind power in their plans for the future (18). Even though

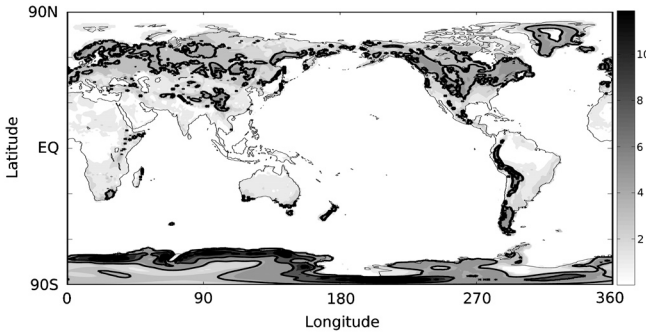


Fig. 5. Mean surface KE dissipation rate (W/m^2) for the 1979–2004 period. Regions demarcated by the black line (3 W/m^2 contour) are ideal for low-impact wind farms.

Downloaded by guest on March 25, 2020

wind currently contributes a small fraction of the total energy consumed by humans, all trends indicate that wind power is on the verge of explosive growth, most of it being in the industrial sector consisting of large wind farms (1). Many of these wind farms are coming up over agricultural land, helping farmers supplement their income with rent from utility companies. Impacts from wind farms on surface meteorological conditions are likely to affect agricultural practices in these farms. In some cases, these impacts may prove to be beneficial, such as the nocturnal warming under stable conditions can protect crops from frosts. If the wind farms are sufficiently large, they may also affect downstream surface meteorology (3). As wind farms become larger and more ubiquitous, it is essential that their possible environmental costs and benefits are assessed and properly addressed to ensure the long-term sustainability of wind power.

Materials and Methods

Observations at San Gorgonio Wind Farm. The San Gorgonio wind farm is located in the northern foothills of the San Jacinto Mountains in California. To avoid effects of mountain-valley winds, observations were collected only when the wind was blowing perpendicular to the slope, i.e, from the northeast to the southwest. The upwind tower was located at 33.896N, 116.604W at an elevation of 290 m. The downwind tower was located at 33.875N, 116.562W, at an elevation of 214 m. The upwind and downwind towers did not record data simultaneously. However, 78% of the pair of observations was recorded within 5 min of each other.

An Aspirated Teledyne-Geotech Model T-210 Pt100 Resistance Temperature Detector was used to measure temperatures at 5 m above ground level sampled at a rate of 5/s. The data were collected using an NEFF Instruments Corporation Model 470 Data Acquisition System. Ten-minute records were continuously recorded except for a 10-min period beginning at local noon when the system performed a self-calibration sequence to remove any dc drift of the temperature and temperature difference channels.

RAMS Model Description and Configuration. We used RAMS, a state-of-the-art regional climate model to simulate the effects of a wind farm. RAMS solved the full three-dimensional, compressible, nonhydrostatic dynamic equations, a thermodynamic equation, and a set of microphysics equations. The system was closed with the Mellor–Yamada level 2.5 scheme (19) that explicitly solves for turbulent kinetic energy while parameterizing other second-order moments. The coordinate system was rectangular Cartesian in the horizontal and terrain-following σ-type (20) in the vertical. We used periodic lateral atmospheric boundary conditions, whereas the bottom boundary conditions were supplied by the Land Ecosystem-Atmosphere Feedback model (21) version 3, dynamically coupled with RAMS.

Using RAMS, we simulated a rectangular 14×6 km domain (Fig. 6), discretized in the horizontal with 1 km spacing. The vertical grid consisted of 18 layers of varying thickness. The lowest three layers were 50, 100, and 100-m thick, respectively. The fourth and higher layers were progressively stretched with a stretch ratio of 1.2 so that the topmost layer reached an altitude of 6,811 m. With eight layers in the lowest 1 km, this vertical grid allowed us to adequately simulate small-scale turbulent processes in the ABL. For simplicity, we assumed the domain to be a flat terrain at sea level.

The simulated wind farm consisted of a 7×3 array of wind turbines. Each turbine was 100-m tall with 50 m rotor blades (100 m rotor diameter), spaced 10 rotor diameters, i.e., 1 km apart. Wind turbine rotors were represented by a subgrid parameterization that assumes a rotor to be an elevated sink of KE and a source of TKE. The parameterization was implemented as follows:

- The turbines occupied 21 grid cells in the center of the model domain with a rotor located in the second atmospheric layer of each grid cell (Fig. 6).
- At each model time step, the volume of air passing through the rotor $\Delta V = \pi R^2 |\vec{U}| \Delta t$, where R = length of rotor blade, $\vec{U}$ = wind velocity in the second atmospheric layer (wind turbine hub height), andΔt = model time step.
- The mass of the said volume of air $\Delta M = \rho \Delta V$, where ρ is the density of air.
- The resolved kinetic energy (RKE) of the air passing through the rotor $\Delta E = \frac{1}{2} \Delta M |\vec{U}|^2$.
- If 2 $ms^{-1} < |\vec{U}| < 20$ ms^{-1}, then 40% of ΔE is removed from the atmospheric flow for generating power. In reality, the energy absorbed by wind turbine rotors is a function of wind speed and rotor design, reaching a maximum of 16/27, known as the Betz Limit (22). The exact form of the function, known as the Coefficient of Performance (C_p), depends on the rotor design. Information on C_p of commercial turbines is proprietary to the manufacturer and is not available in the public domain. C_p can be in the range of 20–55% for most turbines depending on the wind speed, reaching 40% at moderate wind speeds (23). We conducted sensitivity studies with $C_p = 30\%$ and 50% and found that our hypothesis is still valid at these levels.
- Observations from the San Gorgonio wind farm show that the TKE of the air passing through the rotor is approximately 5 m^2 s^{-2} higher than the ambient value and remains fairly constant with varying wind speeds (6). Taylor (24) has reported similar values. Thus, TKE generated in the entire wake due to spinning of the rotor can be represented by $\Delta e = 5 \rho \Delta V$.
- The TKE of the grid cell can now be calculated as $e_1 = e_0 + \frac{\Delta e}{\rho V}$, where e_0 and e_1 are the TKEs of the grid cell before and after the rotor parameterization subroutine is called, respectively, and V is the volume of the grid cell.
- The RKE of the grid cell containing the rotor decreases because a part of it is removed to generate electricity while another part is converted to turbulence in the wake. So, at the end of the time step, the RKE of the grid cell becomes $E_1 = E_0 - 0.4\Delta E - \frac{\Delta e}{\rho V}$, where E_0 and E_1 are the RKEs of the grid cell before and after the rotor parameterization subroutine is called, respectively.
- The wind velocity of the cell can now be calculated as $\vec{U} = \sqrt{\frac{2E_1}{\rho V}}$.

In the Mellor–Yamada closure scheme, TKE and momentum are prognosed. The rotor parameterization effectively adds a source term to the TKE equation and a sink term to the momentum equation. The magnitudes of these source/sink terms are small when averaged over the entire grid cell because the volume of air passing through the rotor is several orders of magnitude smaller than the volume of the grid cell. Thus, although TKE in the wake of a rotor can be large, the average TKE of the grid cell containing that rotor is marginally higher than the ambient. Hence, the source/sink terms do not produce an instantaneous shock to destabilize the system. However, as shown previously, the impacts of these terms can be large when integrated over the entire simulation period.

Our momentum sink/turbulence source parameterization is quite different from the roughness length approach used in studies with general circulation models (GCMs) (2, 3, 5). Our parameterization is particularly appropriate for the RAMS and other flexible mesoscale models where the vertical resolution is adjustable, which allows us to simulate the flow both under and above the turbine hub heights. Most GCM grids are fixed and hence the roughness length approach is the only option. Comparing these two approaches is beyond the scope of this study. However, the simulation results demonstrate that our parameterization is capable of simulating the observed patterns of near-surface air temperatures.

We initialized the model with atmospheric sounding data for November 1, 2008, February 1, May 1, and August 1, 2009, from 21 WMO stations in western United States (Table 2). The data can be accessed online at www.weather.uwyo.edu/upperair/sounding.html. The soundings were available for 0Z and 12Z, corresponding to 4 AM and 4 PM local standard time, respectively. In total, 153 complete soundings were available. For each initial condition, we conducted a pair of numerical simulations with the rotor parameterization switched on and off. The model was integrated for 1 h with a time step of 2 s. These 153 cases cover the entire annual cycle and allowed us to explore how turbine rotors affect near-surface temperatures within the wind farm under a wide range of meteorological conditions.

We used outputs from the ensemble simulations to study how ambient atmospheric flow parameters affect temperature change within the wind farm. The temperature changes were calculated by averaging over the 21

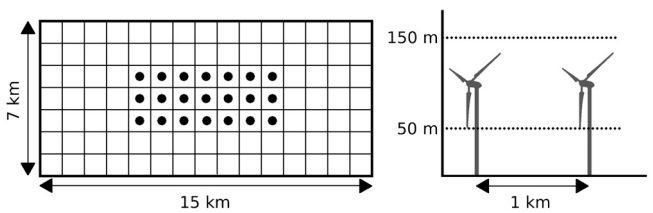


Fig. 6. RAMS model domain. (*Left*) A horizontal cross-section with the dots indicating location of rotors in the second atmospheric layer. (*Right*) The two lowest atmospheric layers with the rotors totally contained within the second layer.

Downloaded by guest on March 25, 2020

grid cells containing the rotors for the entire 1 h simulation period. Ambient flow parameters such as lapse rate, hub-height wind speed, TKE, and surface KE dissipation rate were calculated from the corresponding 21 points in the control simulations that are free from wind farm effects.

Calculating Dissipation from JRA25 Dataset. From Monin–Obukov Similarity (25), the vertical turbulent transfer of momentum between the atmosphere and the surface is given by

$$\overline{(w'V')}_s = -C_m|V_1|V_1,$$

where the subscripts s and 1 stand for surface and lowest atmospheric level, respectively.

The Bulk Richardson Number is given by

$$R_{iB} = \frac{gz_1(\theta_{v1} - \theta_{vs})}{\theta_{v1}|V_1|^2}.$$

From Louis (26), the drag coefficient is

$$C_m = \begin{cases} \frac{\gamma_m}{1+10R_{iB}/\sqrt{1+5R_{iB}}} & R_{iB} > 0 \\ \gamma_m\left[1 - \frac{10R_{iB}}{1+75\gamma_m\sqrt{z_1|R_{iB}|/z_{0m}}}\right] & R_{iB} \le 0 \end{cases}$$

and

$$\gamma_m = \left[\frac{k}{\ln(z_1/z_0)}\right]^2,$$

where V is horizontal wind speed, θ_v is virtual potential temperature, z is height of atmospheric levels, z_0 is surface momentum roughness length, g is acceleration due to gravity, and k is the von Karman constant.

Finally, the surface KE dissipation is calculated as $V_1\overline{(w'V')}_s$.

ACKNOWLEDGMENTS We thank Dr. Neil Kelley of the National Renewable Energy Laboratory for providing the San Gorgonio wind farm data.

1. Wiser R, et al. (2007) *Annual Report on US Wind Power Installation, Costs and Performance Trends: 2006* (US Dept of Energy), pp 9–10.
2. Keith DW, et al. (2004) The influence of large-scale wind power on global climate. *Proc Natl Acad Sci USA* 101:16115–16120.
3. Kirk-Davidoff DB, Keith DW (2008) On the climate impact of surface roughness anomalies. *J Atmos Sci* 65:2215–2234.
4. Sta. Maria MRV, Jacobson MZ (2009) Investigating the effect of large wind farms on energy in the atmosphere. *Energies* 2:816–838.
5. Wang C, Prinn RJ (2010) Potential climatic impacts and reliability of very large-scale wind farms. *Atmos Chem Phys* 10:2053–2061.
6. Baidya Roy S, Pacala SW, Walko RL (2004) Can large wind farms affect local meteorology? *J Geophys Res* 109:D19101 10.1029/2004JD004763.
7. Adams AS, Keith DW (2007) Wind energy and climate: Modeling the atmospheric impacts of wind energy turbines. *EOS Trans AGU* 88 Fall Meeting Suppl.
8. Pielke RA, et al. (1992) A comprehensive meteorological modeling system—RAMS. *Meteorol Atmos Phys* 49:69–91.
9. Cotton WR, et al. (2003) RAMS 2001: Current status and future directions. *Meteorol Atmos Phys* 82:5–29.
10. Stull RB (1993) *An Introduction to Boundary Layer Meteorology* (Kluwer, Dordrecht, The Netherlands) p 2.
11. Stull RB (1993) *An Introduction to Boundary Layer Meteorology* (Kluwer, Dordrecht, The Netherlands), pp 29–32.
12. Onogi K, et al. (2007) The JRA25 reanalyses. *J Meteorol Soc Jpn* 85:369–432.
13. Boer GJ, Lambert S (2008) The energy cycle in atmospheric models. *Clim Dynam* 30:371–390.
14. Lu X, McElroy MB, Kiviluoma J (2009) Global potential for wind-generated electricity. *Proc Natl Acad Sci USA* 106:10933–10938.
15. Ekinton CN, Manwell JF, McGowan JG (2005) Offshore wind farm layout optimization (owflo) project: An introduction. (Copenhagen Offshore Wind Conference, Copenhagen).
16. Lackner MA, van Kuik G (2009) A comparison of smart rotor control approaches using trailing edge flaps and individual pitch control. *Wind Energy* 13:117–134 10.1002/we.353.
17. Pacala SW, Socolow R Stabilization wedges: Solving the climate problem for the next 50 years with current technologies. *Science* 305:968–972.
18. *Global Wind 2008 Report* (Global Wind Energy Council, Brussels).
19. Mellor GL, Yamada T (1982) Development of a turbulence closure model for geophysical fluid problems. *Rev Geophys Space Phys* 20:851–875.
20. Clark TL (1977) A small-scale dynamic model using a terrain-following transformation. *J Comput Phys* 24:186–215.
21. Walko RL, et al. (2000) Coupled atmosphere-biophysics-hydrology model for environmental modeling. *J Appl Meteorol* 39:931–944.
22. Frandsen S (1992) On the wind speed reduction in the center of large clusters of wind turbines. *J Wind Eng Ind Aerod* 39:251–265.
23. Stankovic S, Campbell N, Harries A (2009) *Urban Wind Energy* (Earthscan, London), pp 122–125.
24. Taylor GJ (1983) Wake and performance measurements on the Lawson-Tancred 17 m horizontal-axis windmill. *IEE Proc A* 130:604–612.
25. Stull RB (1993) *An Introduction to Boundary Layer Meteorology* (Kluwer, Dordrecht, The Netherlands), pp 357–358.
26. Louis JF (1979) A parametric model of vertical eddy fluxes in the atmosphere. *BoundLay Meteorol* 17:187–202.

Downloaded by guest on March 25, 2020